Genetic interaction between members of the Vangl family causes neural tube defects in mice

Elena Torban*, Anne-Marie Patenaude*, Severine Leclerc†, Staci Rakowiecki‡, Susan Gauthier*, Gregor Andelfinger†, Douglas J. Epstein‡, and Philippe Gros*§

*Department of Biochemistry, McGill University, Montreal, QC, Canada H3G 1Y6; †Cardiovascular Genetics Unit, Ste-Justine Hospital, Montreal, QC, Canada H3T 1C5; and ‡Department of Genetics, University of Pennsylvania School of Medicine, Philadelphia, PA 19104

Communicated by Louis Siminovitch, Mount Sinai Hospital, Toronto, ON, Canada, January 7, 2008 (received for review November 15, 2007)

Neural tube defects (NTDs) are very frequent congenital abnormalities in humans. Recently, we have documented independent association of *Vangl1* and *Vangl2* gene mutations with NTDs. In the Looptail mouse, homozygosity (but not heterozygosity) for loss-of-function alleles at *Vangl2* causes the severe NTD craniorachischisis, whereas heterozygosity for mutant variants of *VANGL1* is associated with NTDs in a human cohort of sporadic and familial cases. To understand the role of *Vangl1* in normal development, we created a mouse mutant with an inactivating mutation at *Vangl1* (*Vangl1*^{gt}). *Vangl1* shows a dynamic pattern of expression in the developing neural tube and notochord at the time of neural tube closure. *Vangl1*$^{gt/+}$ heterozygotes and *Vangl1*$^{gt/gt}$ homozygotes are viable and fertile, although *Vangl1*$^{gt/gt}$ display subtle alterations in polarity of inner hair cells of the cochlea. Remarkably, and as opposed to healthy *Vangl1*$^{gt/+}$ and *Vangl2*$^{lp/+}$ heterozygotes, *Vangl1*$^{gt/+}$;*Vangl2*$^{lp/+}$ double heterozygotes show profound developmental defects that include severe craniorachischisis, inner ear defects (disorganization of the stereociliary bundles of hair cells of the organ of Corti), and cardiac abnormality (aberrant right subclavian artery). These results show that genetic interaction between *Vangl1* and *Vangl2* genes causes neural tube defects and raise the possibility that interaction between individual *Vangl* genes and other genetic loci and/or environmental factors may additionally contribute to the etiology of NTDs.

convergent extension | Looptail mice | planar cell polarity | mutant mouse

Neural tube defects (NTDs) constitute one of the most common congenital abnormalities in humans, occurring in 1 per 1,000 live births (1). NTDs range across a spectrum of pathologies, from very benign closed spinal dysraphisms, such as dermal sinus, to the severe open dysraphisms, such as myelomeningocele, cephalocele, and craniorachischisis (2, 3). The molecular mechanisms underlying NTDs are complex, with both genetic and environmental contributions. NTDs behave as a complex trait with genetic heterogeneity, incomplete penetrance, and expressivity further modulated by environmental factors, including perinatal supplementation with folic acid (1, 4), all likely to contribute to the wide spectrum of disease. The study of mouse mutants with NTDs has proven useful to identify molecular pathways involved in the complex process of neurulation (5). Looptail (*Lp*) is a semidominant mutation in which *Lp*/+ heterozygotes display urogenital defects and a characteristic "looped" tail. *Lp*/*Lp* homozygotes die *in utero* of a severe NTD, craniorachischisis, a condition in which the neural tube fails to initiate closure and remains completely open from midbrain to tail (6). Additional defects in *Lp*/*Lp* embryos are noticed in the inner ear (organization of hair cells of the cochlea) and the heart (outflow tract defects) (7, 8). *Lp* is caused by mutations in *Vangl2* (9, 10), a gene that codes for a four-transmembrane domain membrane protein (9, 11). During development, Vangl2 is expressed along the neural tube at the time of closure, from the midbrain/hindbrain boundary to its most-caudal extent, decorating the entire neuroepithelial dorsal–ventral axis, including floor plate cells (9, 10, 12).

Vangl2 belongs to a group of highly conserved planar cell polarity (PCP) proteins initially discovered in *Drosophila* (13–15). They include the membrane proteins Frizzled and Van Gogh and the cytoplasmic proteins Dishevelled and Prickle that form membrane-bound signaling complexes (16–24). *Lp*-associated *Vangl2* mutations (*Vangl2*^{E255D}, *Vangl2*^{S464N}) map to the cytoplasmic domain of the protein and abrogate interaction of Vangl2 with Dishevelled (Dvl) (25). Studies of mutants of vertebrate PCP genes show that PCP genes play a role in convergent extension (CE) movements. CE is the process by which cells move mediolaterally and intercalate with each other, causing remodeling of a tissue or epithelium with narrowing in one axis and lengthening in a perpendicular axis. CE plays a role during gastrulation and neurulation and is responsible for narrowing and lengthening the neural plate during neural tube closure (26–30). In mice, PCP failure causes severe NTD, including that detected in *Lp* embryos.

Vertebrates have a second *Vangl* gene, *Vangl1*. Vangl1 and Vangl2 proteins share ≈70% similarity, including identical predicted secondary structures. This structural similarity underlies conserved function: Vangl1 and Vangl2 proteins bind to three mammalian Dvl proteins, and *Lp* mutations engineered in Vangl1 or Vangl2 abrogate interaction with Dvl (25). Likewise, ectopic expression of the zebrafish *Vangl1* relative partly suppress the gastrulation defect of *tri* (*Vangl2*) mutants (31). Although little is known about the role of Vangl1 during development, we have identified independent mutations (V239I, R274Q, M328T) in the human *VANGL1* gene in sporadic and familial cases of NTDs (32). The mutations are patient-specific and affect residues highly conserved in the evolution of the *Vangl* family. *VANGL1*^{V239I} is a *de novo* mutation in a familial setting that abrogates interaction between VANGL1 and members of the Dishevelled family (32). As opposed to the mouse, in which homozygosity for loss-of-function mutations at PCP genes (including *Vangl2*) is both necessary and sufficient for craniorachischisis, human NTD patients have been found to be heterozygote for *VANGL1* mutations. This suggests that these mutations are either dominant negative, cause loss-of-function in a gene dosage-dependent pathway, or may be modulated by lesions at other genetic loci or environmental conditions. To better characterize the role of Vangl1 during embryogenesis and in the etiology of NTDs, we created and studied a mouse mutant bearing a disrupted *Vangl1* gene.

Author contributions: E.T., G.A., D.J.E., and P.G. designed research; E.T., A.-M.P., S.L., S.R., and S.G. performed research; E.T., S.L., S.R., G.A., D.J.E., and P.G. analyzed data; and E.T., G.A., D.J.E., and P.G. wrote the paper.

The authors declare no conflict of interest.

§To whom correspondence should be addressed at: Department of Biochemistry, McGill University, 3655 Drummond, Room 907, Montreal, QC, Canada, H3G 1Y6. E-mail: philippe.gros@mcgill.ca.

This article contains supporting information online at www.pnas.org/cgi/content/full/0712126105/DC1.

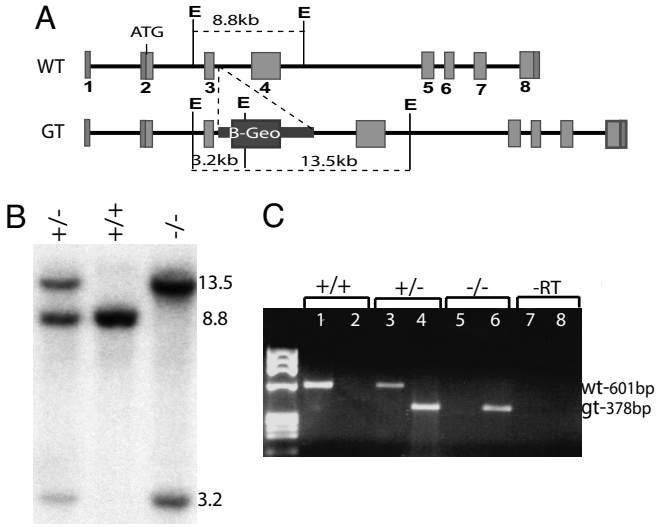

Fig. 1. Generation of the *Vangl1* mutant transgenic mouse line. (*A*) Schematic representation of WT and targeted *Vangl1* alleles, including the inserted β-gal–Neomycin resistance gene-trap cassette. (*B*) WT and targeted *Vangl1* alleles distinguished by Southern blotting of genomic DNA digested with EcoRV (E) and probed with a 601-bp exon 3–4 cDNA probe, which yields fragments of 8.8 kb (WT) vs. 3.2/13.5 kb (targeted). (*C*) Diagnostic RT-PCR to amplify WT (601 bp; lanes 1, 2, 5, and 7) and mutant (378 bp; lanes 2, 4, 6, and 8) *Vangl1* transcripts.

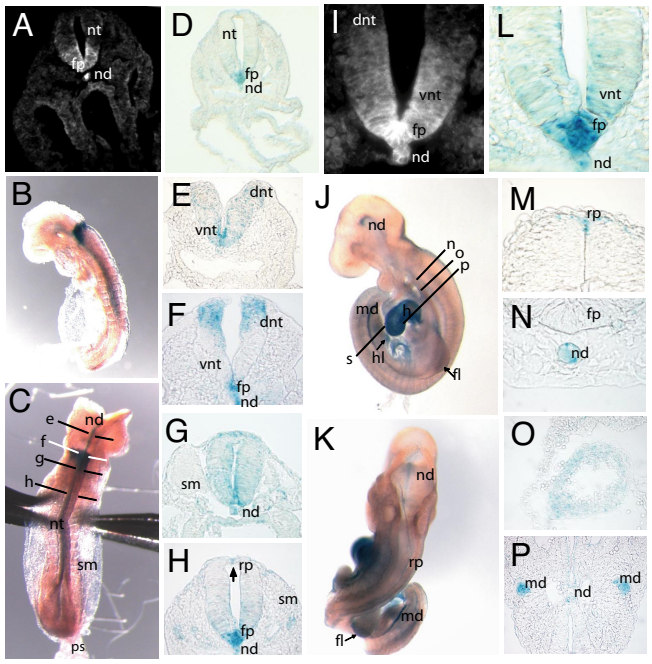

Fig. 2. *Vangl1* expression during neurulation. (*A* and *I*) Detection of Vangl1 protein in E8.5 WT embryos by using a rabbit anti-Vangl1 polyclonal antiserum (magnification, ×200 and ×630). (*B* and *C*) Whole-mount X-gal staining on E8.5 *Vangl1*$^{gt/gt}$ embryos showing lateral and dorsal views, respectively. The section planes used for *E–H* are shown in *C*. (*D* and *L*) Section of *Vangl1*$^{gt/gt}$ E8.5 embryo stained with X-gal showing a pattern of *Vangl1* expression in notochord and floor plate very similar to that detected with anti-Vangl1 antiserum (magnification, ×200 and ×630) (*E–H*). Transverse sections and X-gal staining of neural tube (E8.5) arranged in rostral–caudal progression (magnification, ×400). (*J* and *K*) Whole-mount X-gal staining of Vangl1$^{gt/gt}$ E9.5 embryos; the section planes used for *M–P* are shown in *K*. (*M–P*) X-Gal staining of E9.5 Vangl1$^{gt/gt}$ embryos; transverse sections (magnification, ×400). (*O* and *P*) X-Gal staining of myocardial cells of heart (*O*) and epithelium of mesonephric duct (*P*). fp, floor plate; dnt, dorsal neural tube; h, heart; hl, hindlimb; md, mesonephric duct; nd, notochord; nt, neural tube; ps, primitive streak; rp, roof plate; sm, somites; vnt, ventral neural tube.

Results

***Vangl1* Mutant Mouse Line.** We identified a mutant embryonic stem cell line (*Vangl1*^{gt}) carrying a β-Geo gene-trap cassette (β-gal and neomycin phosphotransferase fusion) inserted into intron 3 of *Vangl1* (GenBank accession no. NC_000069) 237 nucleotides downstream of the exon 3 donor-splice site (Fig. 1*A*). The transcript expressed by the targeted *Vangl1* allele is predicted to code for a severely truncated nonfunctional protein consisting of 63 aa of the N-terminal cytoplasmic portion fused to β-gal. The *Vangl1*^{gt} targeted allele was verified by Southern blotting of EcoRV digested DNA (WT allele, 8.8 kb; mutant, 13.5 kb, 3.2 kb) (Fig. 1*B*). RT-PCR amplification was used to demonstrate expression of both WT and mutant transcripts at a similar level in *Vangl1*$^{gt/+}$ heterozygote mice, whereas only mutant transcripts were detected in *Vangl1*$^{gt/gt}$ homozygotes (Fig. 1*C*). We also tested the possibility that normal splicing of intron 3 might occur in the targeted allele causing excision of the β-Geo cassette and production of WT *Vangl1* mRNA. In a panel of homozygote *Vangl1*$^{gt/gt}$ embryos, a very low level of WT *Vangl1* transcript (<5% of total) was noted by RT-PCR in one animal [supporting information (SI) Fig. 7, *Lower*, embryo no. 2, lane 22]. Thus, insertion of the β-Geo cassette eliminates or severely reduces *Vangl1* expression. Importantly, *Vangl1*$^{gt/gt}$ mutant mice develop normally, have no gross anatomical defects and are otherwise healthy.

Expression of *Vangl1* During Early Development. Production of Vangl1/β-gal fusion by the targeted allele permits evaluation of *Vangl1* expression during development. We first examined the pattern of *Vangl1* transgene expression in neurulating embryos (Fig. 2). X-Gal staining faithfully recapitulated the expression of endogenous Vangl1 protein (detected with anti-Vangl1 antibody) in the floor plate and the notochord (Fig. 2 *A*, *D*, *I*, and *L*). In embryonic day (E)8.0 to E8.5 embryos, a dynamic pattern of X-gal staining was noted along the rostrocaudal axis (Fig. 2 *B*, *C*, and *E–H*). In all sections, Vangl1:β-gal was expressed in the floor plate cells and in the notochord. In rostral hindbrain, strong X-gal staining was noted in the ventral ventricular zone (Fig. 2*E*). At rhombomere 4 (open neural tube), we identified two strong Vangl1:β-gal expression areas in the ventral and dorsal parts of the neural tube (Fig. 2*F*). At the level of closure 1, the entire neural tube cross-section was positive for β-Gal (Fig. 2*G*). Finally, in more caudal regions (closed neural tube), Vangl1:β-Gal expression was found in the floor plate and in a few cells of the roof plate, near the junction point of apposed neural folds (Fig. 2*H*, arrow). Upon completion of neural tube closure at E9.5, most Vangl1:β-gal expression disappeared from the closed neural tube (Fig. 2 *J* and *K*) except for a few cells in the roof plate (Fig. 2*M*). However, Vangl1:β-gal expression remained strong in the notochord, where it persisted through E13.5 (Fig. 2*N*). At E9.5, Vangl1:β-gal expression began to appear outside of the neuroepithelium, notably in the heart (Fig. 2 *J* and *O*), mesonephric ducts (Fig. 2*P*), and limb mesenchyme (arrows in Fig. 2 *J* and *K*). To compare Vangl1 and Vangl2 expression during neural tube closure, E8.5 sections were stained with Vangl1 and Vangl2 antisera (Fig. 3), as we described previously (25). Whereas Vangl1 expression was restricted to the midline floor plate cells and to the notochord (Fig. 3 *A* and *D*), Vangl2 was more widely distributed over the entire neuroepithelium (including some of the Vangl1-positive cells in the floor plate cells) but was absent from the notochord (Fig. 3 *B* and *E*). The identity of notochord and floor plate cells was confirmed by staining with the marker Foxa2 (Fig. 3 *C* and *F*). Together, these results show

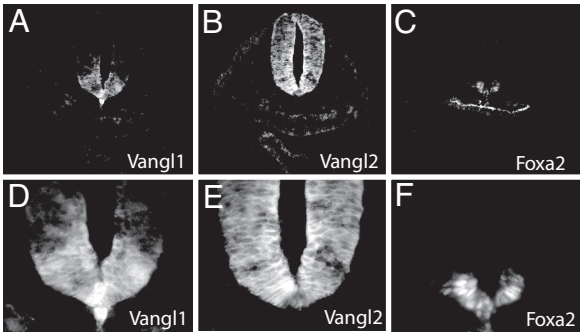

Fig. 3. *Vangl1* and *Vangl2* protein coexpression in neural tube. Serial transverse sections of E8.5 embryos stained with anti-Vangl1 (*A* and *D*), anti-Vangl2 (*B* and *E*), and anti-Foxa2 (*C* and *F*) antisera. Magnification, ×200 (*A–C*); ×630 (*D–F*).

that *Vangl1* mRNA and proteins are expressed in the developing neural tube.

***Vangl1* and *Vangl2* Genetically Interact to Regulate Neural Tube Closure.** Considering that heterozygosity for *VANGL1* mutations is associated with NTDs in humans, the finding that *Vangl1*-null mutant mice develop normally and have no NTD was surprising. Because *Vangl2* and *Vangl1* are structurally related and coexpressed in the developing neural tube, we tested the possibility that the two genes interact during development. When $Vangl1^{gt/gt}$ homozygotes were mated with $Vangl2^{lp/+}$ heterozygotes, ≈20% of the offspring had looped tails, a significant deviation from the 50:50 ratio expected for a fully penetrant *lp* allele. Genotyping at the time of weaning indicated that all normal animals were $Vangl1^{gt/+}$;$Vangl2^{+/+}$, whereas those with looped tails were $Vangl1^{gt/+}$;$Vangl2^{lp/+}$. In 10 $Vangl1^{gt/gt}$ × $Vangl2^{lp/+}$ crosses, >60% of $Vangl1^{gt/+}$;$Vangl2^{lp/+}$ E13.5 to E18.5 embryos (20/32) exhibited craniorachischisis (Fig. 4 *C* and *D*). In Fig. 4 *E* and *F*, the NTD of $Vangl1^{gt/+}$;$Vangl2^{lp/+}$ double heterozygotes was as severe as that of $Vangl2^{lp/lp}$ homozygotes. Therefore, late embryonic lethality is likely responsible for the distorted ratio of $Vangl1^{gt/+}$;$Vangl2^{lp/+}$ double heterozygotes at birth. The surviving $Vangl1^{gt/+}$;$Vangl2^{lp/+}$ pups with looped tails did not display any obvious neural tube defects. The occurrence of craniorachischisis in $Vangl1^{gt/+}$;$Vangl2^{lp/+}$ double heterozygotes establishes that *Vangl1* and *Vangl2* interact genetically during neural tube development.

PCP Defects in the Inner Ear of $Vangl1^{gt/gt}$ and Compound $Vangl1^{gt/+}$;$Vangl2^{lp/+}$ Embryos. In addition to craniorachischisis, PCP mutants display a characteristic planar cell polarity defect in the orientation of stereociliary bundles in hair cells of the organ of Corti (7, 33–35). We detected Vangl1 and Vangl2 protein expression in the organ of Corti (SI Fig. 8) and examined the organ of Corti in E18.5 embryos of various genotypes. We observed a significant reduction in cochlear size in compound $Vangl1^{gt/+}$;$Vangl2^{lp/+}$ heterozygotes exhibiting craniorachischisis (compared with $Vangl1^{gt/+}$;$Vangl2^{+/+}$ controls), similar to that seen in $Vangl2^{lp/lp}$ embryos (Fig. 5*A*). In whole-mount cochlear preparations from $Vangl1^{gt/+}$ heterozygotes and $Vangl1^{gt/gt}$ homozygotes, we observed that: (*i*) the number and organization of hair cell rows was undisturbed in $Vangl1^{gt/gt}$ mutants; (*ii*) there was a modest but significant misorientation of stereociliary bundles in all hair cell layers of $Vangl1^{gt/gt}$ embryos (±30–90° in either direction) (SI Fig. 9). Significantly, $Vangl1^{gt/+}$;$Vangl2^{lp/+}$ embryos had profound distortion of stereociliary bundles, although the distribution of affected cell layers was different from that detected in $Vangl2^{lp/lp}$ mice (Fig. 5 *B* and *C*). At the base of the cochlear duct, 20% of the inner hair cells (IHCs) were misoriented (compared with 70% in $Vangl2^{lp/lp}$ tissues). Misorientation of all three outer hair cell (OHC) layers was seen in compound heterozygotes, particularly at the apical turn: >50% in OHC1, 65% in OHC2, and >80% in OHC3. The stereociliary vertices were randomly oriented, with rotation angles of 40–180°, similar to $Vangl2^{lp/lp}$ cochleas. Therefore, *Vangl1* and *Vangl2* genetically interact to regulate planar polarity in the inner ear, including orientation of stereociliary bundles, extension of cochlear ducts, and thinning of cell layers that position hair cells in organized rows.

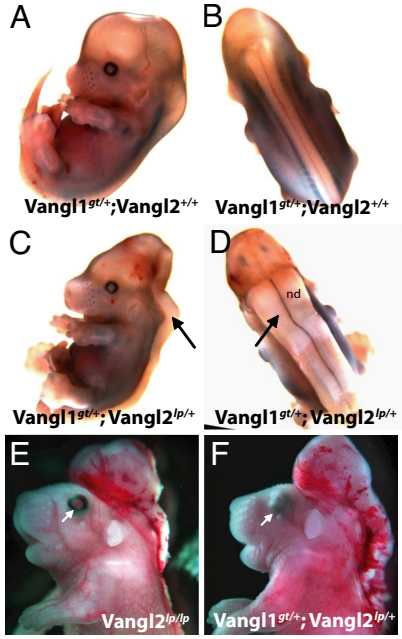

Fig. 4. Genetic interaction between *Vangl1* and *Vangl2* during neural tube closure. The presence of craniorachischisis in $Vangl2^{lp/lp}$ (*E*) and in $Vangl1^{gt/+}$;$Vangl2^{lp/+}$ double heterozygote embryos (arrows in *C* and *D*) is compared with phenotypically normal $Vangl1^{gt/+}$;$Vangl2^{+/+}$ controls (*A* and *B*). E13.5 embryos are shown in *A–D*. E18.5 embryos are shown in *E* and *F*. *B* and *D* are dorsal views of embryos in *A* and *C*. Closed vs. open eyelid is identified by white arrows in *E* and *F*.

Cardiac Defects in Compound $Vangl1^{gt/+}$;$Vangl2^{lp/+}$ Embryos. In addition to craniorachischisis, $Vangl2^{lp/lp}$ mice have severe cardiac anomalies, including double-outlet right ventricles, ventricular septal defects, and malposition of the great arteries (36). $Vangl1^{gt/gt}$ embryos had *Vangl1*:β-gal gene expression in heart tissue from E9.5 onward (Figs. 2 and 6 *A* and *B*). No cardiac outflow abnormalities were detected in $Vangl1^{gt/+}$;$Vangl2^{lp/+}$ double heterozygotes or in $Vangl^{gt/gt}$ homozygotes, although intracardiac defects were regularly seen in $Vangl2^{lp/lp}$ embryos (data not shown). Examination of aortic arch structures in $Vangl1^{gt/+}$;$Vangl2^{lp/+}$ embryos identified an aberrant right subclavian artery, which was confirmed by 3D reconstruction analysis as compared with WT (Fig. 6 *G* and *F*). The same extracardiac phenotype was evident in $Vangl2^{lp/lp}$ embryos (Fig. 6*D*). The right subclavian artery originates from the fourth aortic arch, which itself is derived from the posterior–medial aspect of the distal aortic arch. We identified X-gal/*Vangl1* staining in the fourth aortic arch (Fig. 6*A*), consistent with the aortic arch anomaly we observed. Detection of the same extracardiac defect in $Vangl1^{gt/+}$;$Vangl2^{lp/+}$ and $Vangl2^{lp/lp}$ embryos suggests that the two genes genetically interact to regulate the proper development of the extracardiac structures.

GENETICS

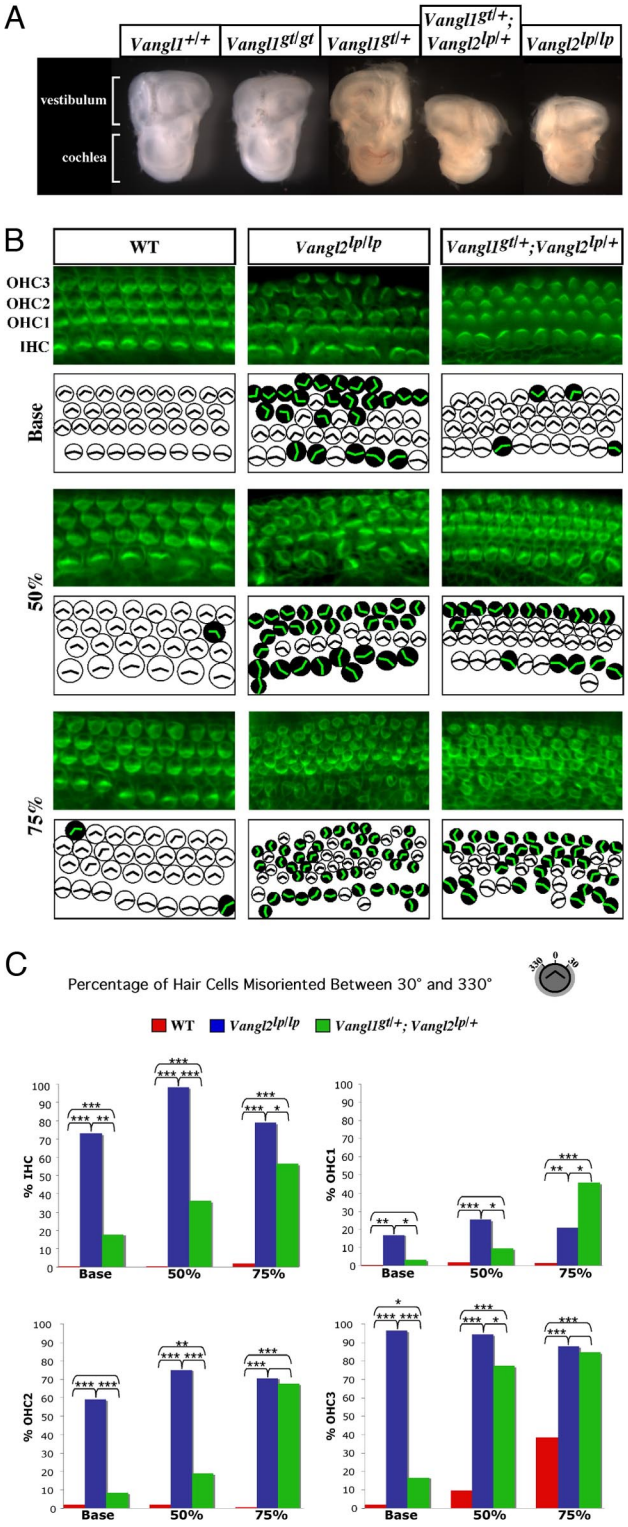

Fig. 5. Genetic interaction of *Vangl1* and *Vangl2* in planar cell polarity of the neurosensory cells in the inner ear. (*A*) Macroanatomy of inner ear structures dissected from E18.5 embryos of various *Vangl1* and *Vangl2* genotypes is shown. (*B*) Whole-mount preparations of organs of Corti from E18.5 WT, $Vangl2^{lp/lp}$, and $Vangl1^{gt/+}$;$Vangl2^{lp/+}$ embryos stained with phalloidin–FITC antibody to visualize actin-based stereociliary bundles. The analyzed regions were determined relative to the length of the cochlear duct. The base region was 5% from the most basal position of the cochlea, the 50% region was the midpoint between the most basal and most apical ends, and the apical region was at 75% from the most basal position. Each microscopic image is schematically depicted: White circles correspond to the hair cells with normal planar orientation of the stereociliary bundles, and the black circles correspond to the hair cells with randomized orientation of the actin vertexes. The individual layers of IHCs and OHCs (OHC1–3) are identified. (*C*) Quantification of the number of misoriented hair cells (as a percentage) found in embryos of different *Vangl1* and *Vangl2* genotypes. The asterisks indicate the level of significance (χ^2 analysis): ***, $P < 0.0005$; **, $P \geq 0.0005$ to $P < 0.005$; *, $P \geq 0.005$ to $P < 0.05$. The absence of an asterisk indicates lack of significance ($P \geq 0.05$).

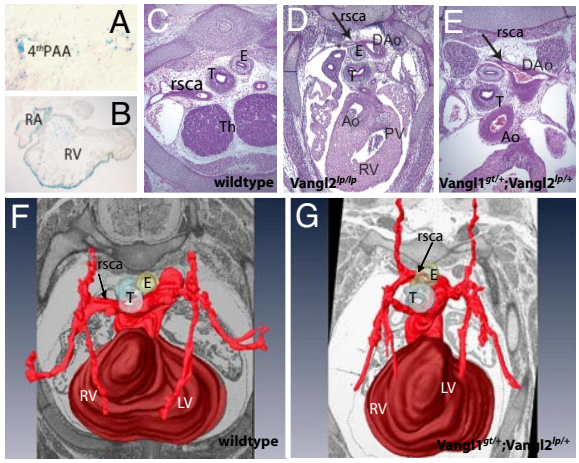

Fig. 6. $Vangl1^{gt/+}$;$Vangl2^{lp/+}$ embryos exhibit aberrant right subclavian artery. (*A*) *Vangl1* expression in fourth aortic arch of E10.5 $Vangl1^{gt/gt}$ embryo (X-gal staining; magnification, ×600). (*B*) X-Gal staining of the intracardiac structures of the of E10.5 $Vangl1^{gt/gt}$ embryos (magnification, ×200). (*C* and *D*) Transverse sections through the hearts of E14.5 embryos (magnification, ×400). (*C*) In WT embryos, the right subclavian artery (arrows) is positioned laterally from trachea and esophagus. In $Vangl2^{lp/lp}$ embryos (*D*) and in $Vangl1^{gt/+}$;$Vangl2^{lp/+}$ (*E*), the right subclavian artery is positioned dorsal to esophagus. (*F* and *G*) Three-dimensional reconstruction of the arteries of E14.5 WT (*F*) and $Vangl1^{gt/+}$;$Vangl2^{lp/+}$ hearts (*G*). Ao, aorta; DAo, dorsal aorta; E, esophagus; LV, left ventricle; PAA, pharyngeal arch artery; PV, pulmonary valve; RA, right atrium; rsca, right subclavian artery; RV, right ventricle; T, trachea; Th, thymic primordium.

Discussion

Murine relatives of fly PCP genes have been shown to participate in the establishment of polarity in certain structures and are important for CE movements during embryogenesis. Initially demonstrated in the Looptail ($Vangl2^{-/-}$) mouse, mutations in other PCP genes including *Dvl*, *Fz*, and *Celsr1* cause craniorachischisis (34, 35, 37). Mammals have a second *Vangl* gene, *Vangl1*. Although its function remains unknown, *VANGL1* mutations are associated with NTDs in humans (32). Here, we created a mouse *Vangl1* mutant. By using β-gal from the trapped $Vangl1^{gt}$ allele as a reporter, *Vangl1* expression was found in the developing neural tube, where it was confined to the floor plate and notochord. In contrast, Vangl2 expression was more abundant and broadly distributed with some overlap with *Vangl1* in the floor plate, whereas notochord was solely positive for Vangl1. Vangl1 and Vangl2 were coexpressed in the cochlea, heart, skin, and kidneys. Although $Vangl1^{gt/+}$ heterozygotes and $Vangl1^{gt/gt}$ homozygotes appeared normal, we noticed a modest but reproducible disorganization of stereociliary bundles in cochlear hair cells of $Vangl1^{gt/gt}$ homozygotes, a first indication for a role of *Vangl1* in PCP. Additional analyses of $Vangl1^{gt/+}$;$Vangl2^{lp/+}$ double heterozygotes identified a striking set of abnormalities, which included (*i*) craniorachischisis, (*ii*) severe misorientation of cochlear stereociliary bundles (both similar to $Vangl2^{lp/lp}$), and (*iii*) a cardiac defect in the form of aberrant right subclavian arteries.

These results demonstrate that *Vangl1* participates in PCP and CE movements in vertebrates, including formation of the neural tube.

In $Vangl1^{gt/+}$;$Vangl2^{lp/+}$ embryos, the extracardiac anomaly (aberrant right subclavian artery) occurred in the absence of intracardiac defects, which are routinely seen in $Vangl2^{lp/lp}$ or $Dvl2^{-/-}$ embryos (36, 37). Lack of outflow tract defects in $Vangl1^{gt/+}$;$Vangl2^{lp/+}$ mutants may be attributable to a lesser sensitivity of myocardial cells to PCP cues or dosages of PCP proteins. Alternatively, Vangl2, like Dvl2, may function in cellular events pertinent specifically to heart development.

NTDs are a heterogeneous set of conditions ranging from very benign to very severe and lethal *in utero*. Although, a clear genetic component to NTD has been documented, this genetic contribution is complex and multigenic, with further modulation of penetrance and expressivity by additional genetic loci and environmental factors (1). Recently, we identified mutations (V239I, R274Q, M328T) in the human *VANGL1* gene in a cohort of 165 patients representing sporadic and familial cases of NTDs. Two of these variants (V239I, M328T) were shown to cause partial or complete loss of *VANGL1* function in complementation studies in zebrafish and Dvl protein interactions in yeast (32). The observations that (*i*) only a small proportion of NTD patients examined harbored mutations in *VANGL1*, (*ii*) all mutations in NTD patients were detected as heterozygotes, and (*iii*) patients with the same *de novo* mutation (V239I) showed different disease severity in a familial setting suggest heterogeneity in the genetic components of NTDs in humans with incomplete penetrance of *VANGL1* mutations. These findings further suggest that in addition to *VANGL1* mutations, environmental factors and/or sensitizing genetic lesions play an important role in the etiology of NTDs in humans. Results from the present study demonstrate that partial loss of *VANGL2* function could be one such sensitizing event.

Although $Vangl1^{gt/+}$;$Vangl2^{lp/+}$ double heterozygotes display craniorachischisis similar to that of $Vangl2^{lp/lp}$, the absence of a neural tube phenotype in $Vangl1^{gt/gt}$ is puzzling. Genetic interactions between *Vangl2* and other PCP genes such as *Ptk7* and Scribble have been shown to cause NTD and inner ear phenotypes in double heterozygotes, but homozygosity for loss-of-function alleles at each of these two loci also causes severe craniorachischisis (38, 39). Whether *Vangl1* genetically interacts with other PCP genes is unknown. Our results suggest a different type of functional relationship between *Vangl1* and *Vangl2*. We propose that the Vangl pathway is exquisitely sensitive to gene dosage during NT formation, with a minimum threshold level of combined Vangl activity required for neural tube closure. We further suggest that Vangl1 and Vangl2 have redundant function. In cells that express abundant levels of Vangl2 compared with Vangl1, Vangl2 may play a seemingly "dominant" role. In this scenario, loss of 50% of Vangl2 puts the pathway in a "sensitized" mode eliciting a phenotype from partial loss of Vangl1. In cells with high levels of Vangl2, loss of Vangl1 may be completely masked or may have a subtle effect (e.g., misorientation of cochlear stereociliary bundles). This model is compatible with the observations that the PCP pathway is highly gene-dosage-dependent, with both loss-of-function mutations and overexpression of individual PCP members resulting in the same deleterious phenotype. Finally, in view of the observation that *VANGL1* mutations in human cases of NTDs were heterozygote, it is tempting to speculate that these do not behave as dominant negative or gain-of-function mutations but rather as partial loss of function in a gene-dosage-dependent pathway that can be further enhanced or attenuated by polymorphic variants at other loci and/or environmental influences. This proposal is also compatible with the broad spectrum of severity and phenotypic manifestations of NTDs in humans.

In conclusion, our observations strongly suggest that VANGL1 functions in the mammalian PCP pathway, acting in concert with VANGL2 to control neural tube formation, orientation of the stereociliary bundles in cochlea, and organization of major extracardiac vessels.

Materials and Methods

Generation of *Vangl1* Mutant Mice. A mouse 129/Ola XL802 ES cell line bearing a gene-trap insertion within mouse *Vangl1* gene ($Vangl1^{gt}$) was obtained (BayGenomics) and injected in C57BL/6J blastocysts. Chimeras were mated to C57BL/6J females and $Vangl1^{gt/+}$ heterozygotes were intercrossed to produce $Vangl1^{gt/gt}$. $Vangl2^{lp/lp}$ embryos were obtained by brother:sister mating of a $Vangl2^{lp/+}$ Looptail stock.

Genotyping. The $Vangl1^{gt}$ allele was detected by EcoRV digestion of genomic DNA and Southern blotting by using a 601bp *Vangl1* cDNA probe generated by RT-PCR by using primer pairs Vangl1–Ex3-F (5′-AGAACAAGAGAAAGACACAAATCAC-3′) and mVangl1–Ex4-R (5′-CTGCGTATTGCACGATGTCC-3′). PCR genotyping was done by using three primers in one reaction: mVangl1–Ex3-F and either Vangl1–In3-R2 (5′-CACCAGATTTCCATGCTTGCCA-3′) (744-bp WT fragment) or GT1-R (5′- CATACTTTCGGTTCCTCTTCCCATG-3′) (410-bp mutant fragment). The $Vangl2^{S464N}$ *Lp* allele was identified by amplification of exon 8 by using primers mVangl2–Ex8-F (5′-ACCTTAGAAACACCCTAGCT-3′) and mVangl2–Ex8-R (5′-ACAGAGGTCTCCGACTGCAGC-3′), followed by nucleotide sequencing.

RNA Preparation and RT-PCR. cDNA was synthesized from RNA by using Maloney murine leukemia virus reverse transcriptase and used to amplify fragments corresponding to either WT (*Vangl1*; 601 bp) or fusion transcript (*Vangl1*–β-Geo; 378 bp), with primers Vangl1–Ex3-F/mVangl1–Ex4-R (WT) and mVangl1–Ex3-F/Pr2-Geo (5′-ATTCAGGCTGCGCAACTGTTGGG-3′) (mutant).

Histology and Immunohistochemistry. Whole-mount staining for β-gal activity was done as described (12). Images from 12-μm X-gal-stained cryosections were acquired by using the AxioVision 4.3 software package (Zeiss). Rabbit anti-Vangl1 and anti-Vangl2 antisera (1:200 and 1:50) (25), mouse anti-Foxa2 (1:20, Developmental Studies Hybridoma Bank, University of Iowa), Cy3-conjugated goat anti-rabbit (Jackson ImmunoResearch), and Alexa Fluor 488-conjugated goat anti-mouse (Invitrogen) were used for immunofluorescence on cryosections. For histology, 5-μm serial sections of fixed embryos or microdissected hearts were stained with hematoxylin/phloxin/saffron. Three-dimensional reconstructions were created by using Amira4.1 software (Mercury Computer Systems) as described previously (40).

Whole-Mount Inner Ear Preparations and Analysis of the Stereocilia Rotation. Cochleas from E18.5 embryos were fixed in 4% paraformaldehyde, microdissected, and incubated with anti-myosin VIIa antibody (1:500; Proteus Biosciences Inc) and Alexa Fluor 488-conjugated phalloidin (1:40), followed by Cy3-conjugated goat anti-rabbit antibody (1:200). The orientation of stereocilia was determined as described (7). A minimum of 40 cells per region per embryo were counted. The stereociliary bundle orientation was determined in relation to a line perpendicular to the pillar cells; cells with a rotation degree of more than 30 in either direction from the perpendicular line were considered misoriented (7).

ACKNOWLEDGMENTS. This work was supported by research grants from the Canadian Institutes of Health Research (to P.G. and G.A.). Work in the laboratories of D.J.E. and G.A. was supported by National Institutes of Health Grant NS39421 and the Canadian Heart and Stroke Foundation, respectively. P.G. is a James McGill Professor of Biochemistry.

1. Frey L, Hauser WA (2003) Epidemiology of neural tube defects. *Epilepsia* 44(Suppl) 3:4–13.
2. Botto LD, Moore CA., Khoury MJ, Erickson JD (1999) Neural-tube defects. *N Engl J Med* 341:1509–1519.
3. Kibar Z, Capra V, Gros P (2007) Toward understanding the genetic basis of neural tube defects. *Clin Genet* 71:295–310.
4. Finnell RH, Waes JG, Eudy JD, Rosenquist TH (2002) Molecular basis of environmentally induced birth defects. *Annu Rev Pharmacol Toxicol* 42:181–208.
5. Copp AJ, Greene ND, Murdoch JN (2003) The genetic basis of mammalian neurulation. *Nat Rev Genet* 4:784–793.
6. Strong LC, Hollander WF (1949) Hereditary loop-tail in the house mouse accompanied by inperforate vagina and with lethal craniorachischisis when homozygous. *J Hered* 40:329–334.

7. Montcouquiol M, *et al.* (2003) Identification of Vangl2 and Scrb1 as planar polarity genes in mammals. *Nature* 423:173–177.
8. Phillips HM, Murdoch JN, Chaudhry B, Copp AJ, Henderson DJ (2005) Vangl2 acts via RhoA signaling to regulate polarized cell movements during development of the proximal outflow tract. *Circ Res* 96:292–299.
9. Kibar Z, Vogan KJ, Groulx N, Justice MJ, Underhill DA, Gros P (2001) Ltap, a mammalian homolog of *Drosophila* Strabismus/Van Gogh, is altered in the mouse neural tube mutant Loop-tail. *Nat Genet* 28:251–255.
10. Murdoch JN, Doudney K, Paternotte C, Copp AJ, Stanier P (2001) Severe neural tube defects in the loop-tail mouse result from mutation of Lpp1, a novel gene involved in floor plate specification. *Hum Mol Genet* 10:2593–2601.
11. Kibar Z, *et al.* (2001) Identification of a new chemically induced allele (Lp(m1Jus)) at the loop-tail locus: Morphology, histology, and genetic mapping. *Genomics* 72:331–337.
12. Torban E, *et al.* (2007) Tissue, cellular and sub-cellular localization of the Vangl2 protein during embryonic development: Effect of the Lp mutation. *Gene Expr Patterns* 7:346–354.
13. Taylor J, Abramova N, Charlton J, Adler PN (1998) Van Gogh: A new *Drosophila* tissue polarity gene. *Genetics* 150:199–210.
14. Wolff T, Rubin GM (1998) Strabismus, a novel gene that regulates tissue polarity and cell fate decisions in *Drosophila*. *Development* 125:1149–1159.
15. Jenny A, Mlodzik M (2006) Planar cell polarity signaling: a common mechanism for cellular polarization. *Mt Sinai J Med* 73:738–750.
16. Klingensmith J, Nusse R, Perrimon N (1994) The *Drosophila* segment polarity gene dishevelled encodes a novel protein required for response to the wingless signal. *Genes Dev* 8:118–130.
17. Theisen H, *et al.* (1994) Dishevelled is required during wingless signaling to establish both cell polarity and cell identity. *Development* 120:347–360.
18. Adler PN, Charlton J, Liu J (1998) Mutations in the cadherin superfamily member gene dachsous cause a tissue polarity phenotype by altering frizzled signaling. *Development* 125:959–968.
19. Chae J, *et al.* (1999) The *Drosophila* tissue polarity gene starry night encodes a member of the protocadherin family. *Development* 126:5421–5429.
20. Gubb D, *et al.* (1999) The balance between isoforms of the prickle LIM domain protein is critical for planar polarity in *Drosophila* imaginal discs. *Genes Dev* 13:2315–2327.
21. Usui T, *et al.* (1999) Flamingo, a seven-pass transmembrane cadherin, regulates planar cell polarity under the control of Frizzled. *Cell* 98:585–595.
22. Feiguin F, Hannus M, Mlodzik M, Eaton S (2001) The ankyrin repeat protein Diego mediates Frizzled-dependent planar polarization. *Dev Cell* 1:93–101.
23. Yang CH, Axelrod JD, Simon MA (2002) Regulation of Frizzled by fat-like cadherins during planar polarity signaling in the *Drosophila* compound eye. *Cell* 108:675–688.
24. Jenny A, Reynolds-Kenneally J, Das G, Burnett M, Mlodzik M (2005) Diego and Prickle regulate Frizzled planar cell polarity signalling by competing for Dishevelled binding. *Nat Cell Biol* 7:691–697.
25. Torban E, Wang HJ, Groulx N, Gros P (2004) Independent mutations in mouse Vangl2 that cause neural tube defects in looptail mice impair interaction with members of the Dishevelled family. *J Biol Chem* 279:52703–52713.
26. Wallingford JB, *et al.* (2000) Dishevelled controls cell polarity during *Xenopus* gastrulation. *Nature* 405:81–85.
27. Jessen JR, *et al.* (2002) Zebrafish trilobite identifies new roles for Strabismus in gastrulation and neuronal movements. *Nat Cell Biol* 4:610–615.
28. Goto T, Keller R (2002) The planar cell polarity gene strabismus regulates convergence and extension and neural fold closure in *Xenopus*. *Dev Biol* 247:165–181.
29. Wallingford JB, Harland RM (2002) Neural tube closure requires Dishevelled-dependent convergent extension of the midline. *Development* 129:5815–5825.
30. Carreira-Barbosa F, *et al.* (2003) Prickle 1 regulates cell movements during gastrulation and neuronal migration in zebrafish. *Development* 130:4037–4046.
31. Jessen JR, Solnica-Krezel L (2004) Identification and developmental expression pattern of van gogh-like 1, a second zebrafish strabismus homologue. *Gene Expr Patterns* 4:339–344.
32. Kibar Z, *et al.* (2007) Mutations in VANGL1 associated with neural-tube defects. *N Engl J Med* 356:1432–1437.
33. Montcouquiol M, *et al.* (2006) Asymmetric localization of Vangl2 and Fz3 indicate novel mechanisms for planar cell polarity in mammals. *J Neurosci* 26:5265–5275.
34. Curtin JA, *et al.* (2003) Mutation of Celsr1 disrupts planar polarity of inner ear hair cells and causes severe neural tube defects in the mouse. *Curr Biol* 13:1129–1133.
35. Wang Y, Guo N, Nathans J (2006) The role of Frizzled3 and Frizzled6 in neural tube closure and in the planar polarity of inner-ear sensory hair cells. *J Neurosci* 26:2147–2156.
36. Henderson DJ, *et al.* (2001) Cardiovascular defects associated with abnormalities in midline development in the Loop-tail mouse mutant. *Circ Res* 89:6–12.
37. Hamblet NS, Lijam N, Ruiz-Lozano P, Wang J, Yang Y (2002) Dishevelled 2 is essential for cardiac outflow tract development, somite segmentation and neural tube closure. *Development* 129:5827–5838.
38. Murdoch JN, *et al.* (2001) Circletail, a new mouse mutant with severe neural tube defects: Chromosomal localization and interaction with the loop-tail mutation. *Genomics* 78:55–63.
39. Lu X, *et al.* (2004) PTK7/CCK-4 is a novel regulator of planar cell polarity in vertebrates. *Nature* 430:93–98.
40. Soufan AT, *et al.* (2004) Reconstruction of the patterns of gene expression in the developing mouse heart reveals an architectural arrangement that facilitates the understanding of atrial malformations and arrhythmias. *Circ Res* 95:1207–1215.